Thermally Activated Delayed Fluorescence in 2-Methyl-5-(Penta(9-carbazolyl)phenyl)-3,4,5-Oxadizole Derivatives.

Matthew W. Cooper,[†] Xiaoqing Zhang,[‡] Yadong Zhang,[†,||,¶] Ajith Ashokan,[§] Canek Fuentes-Hernandez,[‡] Seyhan Salman,[§] Bernard Kippelen,[‡,*] Stephen Barlow,[†,||,*] Seth R. Marder[†,||,¶,*].

† Center for Organic Photonics and Electronics and School of Chemistry and Biochemistry, Georgia Institute of Technology, Atlanta, GA 30332, USA.

‡ Center for Organic Photonics and Electronics and School of Electrical and Computer Engineering, Georgia Institute of Technology, Atlanta, GA 30332, USA.

|| Renewable and Sustainable Energy Institute (RASEI), University of Colorado Boulder, Boulder, CO 80303, USA.

§ Chemistry Department, Clark Atlanta University, Atlanta, GA 30314, USA.

¶ Department of Chemical and Biological Engineering and Department of Chemistry, University of Colorado Boulder, Boulder, CO 80309, USA.

ABSTRACT: 2,5-Diphenyl-1,3,4-oxadiazole has been widely used as an acceptor portion of donor-acceptor fluorophores that exhibit thermally activated delayed fluorescence (TADF), but analogous 2-alkyl-5-phenyl-1,3,4-oxadiazoles have been much less widely investigated. Here the properties of carbazole-substituted 2-methyl-5-phenyl-1,3,4-oxadiazoles are compared to those of their 2,5-diphenyl analogues; the fluorescence of each of the former compounds is blue shifted by ca. 50-100 meV relative to those in the latter, while maintaining similar values of the singlet–triplet energy separation, ΔE_{ST}. In particular 2-methyl-5-(penta(9-carbazolyl))-1,3,4-oxadiazole and 2-methyl-5-(penta(3,6-di-*tert*-butyl-9-carbazolyl))-1,3,4-oxadiazole exhibit solution fluorescence maxima of 466 and 485 nm, respectively, and estimated ΔE_{ST} values of 0.12 and 0.03 eV. In both cases the reverse intersystem crossing rates inferred from their solution fluorescence behavior are over twice those of the corresponding 2-phenyl derivatives. Organic light-emitting diodes (OLEDs) in which the 2-methyl derivatives are used as emitters yield external quantum efficiency (EQE) values of up to 23%. OLEDs with 2-methyl-5-(penta(9-carbazolyl))-1,3,4-oxadiazole and 2-methyl-5-(penta(3,6-di-*tert*-butyl-9-carbazolyl))-1,3,4-oxadiazole emitters show reduced efficiency roll off at high current densities relative to their 2-phenyl counterparts, the latter exhibiting an EQE of 16% at 1000 cd m^{-2}.

INTRODUCTION

Molecules that exhibit efficient thermally activated delayed fluorescence (TADF) have attracted considerable interest as emitters in organic light-emitting diodes as they can potentially afford electroluminescent devices with 100% internal quantum efficiency.[1-5] Such fluorophores are generally molecules based on weakly coupled donor and acceptor moieties. To obtain efficient blue emission, donor and acceptor moieties should have appropriate donor and acceptor strengths to achieve a charge-transfer singlet excited state (^{1}CT) that is sufficiently high in energy and that exhibits efficient photoluminescence (PL). In addition, the locally excited triplet states (^{3}LE) associated with donor and acceptor units should be sufficiently high in energy that they do not compromise the energy separation between the lowest lying singlet (S_1) and triplet (T_1) excited states (ΔE_{ST}). As well as a small value of ΔE_{ST}, spin-orbit coupling (SOC) also plays an important role in facilitating reverse intersystem crossing (RISC);[6] SOC is stronger in systems where the relevant triplet state – either T_1 or an energetically accessible T_n state that facilitates RISC *via* a spin-vibronic coupling mechanism – has different orbital character from S_1.[7]

The 2,5-diphenyl-1,3,4-oxadiazole acceptor moiety (**DPO**, Chart 1) has good thermal stability and high PL quantum yield (Φ_{PL}), and can be readily modified to create a diverse set of derivatives; accordingly this moiety has been widely used in OLEDs as a component of electron-transport materials,[8-11] host materials for phosphorescent emitters,[12-17] and donor-acceptor TADF emitters.[18-26] However, the ^{3}LE energy of the **DPO** unit (ca. 3.3-3.4 eV from the high-energy onset of phosphorescence for **DPO** itself,[12] ca. 2.6-2.7 eV when linked to carbazoles, which are probably the most widely used donors in TADF emitters,[27] and similar donors[15-18,22]) limits its applicability as both a host and TADF emitter for the bluest emitting devices. This triplet energy could be raised by shortening the conjugation length of the acceptor, through replacement of one of the phenyl groups with a hydrogen atom or an alkyl group, as in the case of 2-methyl-5-phenyl-1,3,4-oxadiazole (**MPO**, Chart 1), or by substitution of one of the phenyl groups in such a way to force it out of conjugation with the oxadiazole. At the same time, the reduced conjugation is also expected to reduce the acceptor strength and lead to a blue shift of the ^{1}CT state. Chart 1 shows the structures of pairs of carbazolyl derivatives of **DPO** and **MPO** that have been compared in the

literature. A previous comparison of the optical properties of **CzDPO**, **CzMPO**, and **CzDPO** derivatives with bulky *o,o*-substitution of the terminal phenyl ring confirm the expectations described above.[18] The dicarbazolyl/bis(oxadiazole) architectures shown in Chart 1 have also been compared for Me, Ph, and other aryl substituents; again the methyl derivative exhibited blue-shifted emission.[19,23]

Chart 1. Structures of DPO, MPO, and Previously Reported Derivatives Discussed in the Introduction.[18,19.,21,23]

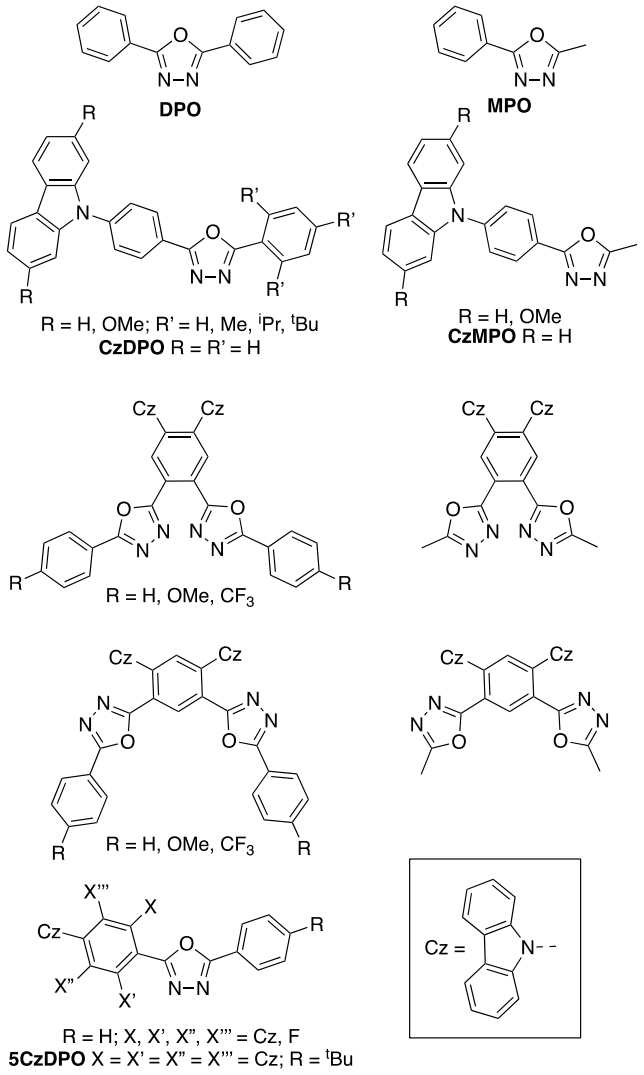

We have recently reported derivatives of **DPO** of the type shown at the bottom left of Chart 1, in which one of the phenyl groups is substituted with various numbers of carbazole donors, and the remaining positions are fluorinated.[21] Of these compounds the pentacarbazolyl derivative, **5CzDPO** (which we synthesized with a 4-*tert*-butyl substituent on the phenyl ring, but for which the corresponding derivative with unsubstituted and CF_3-substituted phenyl groups have also also been reported[20,26]), afforded a low ΔE_{ST} (estimated from the onset of room-temperature solution steady-state PL and that of delayed PL at 77 K) of 0.12 eV, as well as the highest device efficiencies of the series, although it also exhibited the one of the longest wavelength PL maxima. We were interested in the extent to which the photophysical properties of **5CzDPO**-type structures could be modified by reduction of the acceptor conjugation length in the manner described above.

Here we report a comparison of **5CzDPO** to its new methyl analogue, **5CzMPO** (Chart 2). We also compare these two compounds to **5*t*CzDPO** and **5*t*CzMPO** (Chart 2), in which the carbazole-9-yl donors are replaced by 3,6-di-*tert*-butylcarbazol-9-yl donors. We find that in the **MPO** derivatives, both S_1 and T_1 energy are raised without increasing ΔE_{ST}, and comparable values of Φ_{PL} can be maintained. Furthermore, the RISC rate constant, k_{RISC}, is also increased. OLEDs fabricated using the **MPO** compounds as the emitter doped into the emissive layer displayed high EQEs in which the efficiency roll-off at high luminance is reduced relative to that for devices incorporating their **DPO** counterparts.

Chart 2. Structures of the Pentacarbazolylphenyl-Oxadiazole Compounds Studied in This Week.

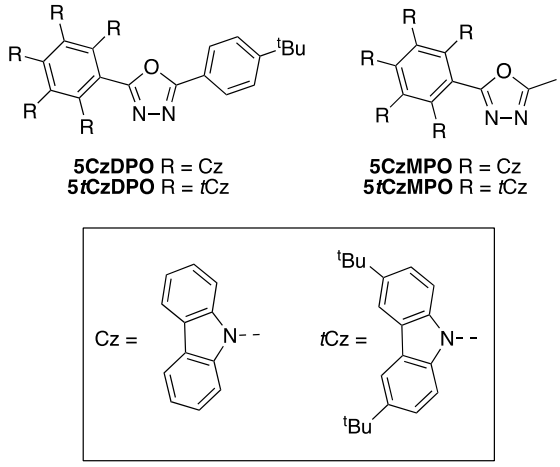

EXPERIMENTAL AND THEORETICAL METHODS

General Considerations. All reagents were purchased from commercial sources and were used without further purification. **5CzDPO** was synthesized as previously described.[21] Other syntheses are described below and shown in Scheme 1. ^{1}H, ^{13}C, and ^{19}F NMR spectra were recorded using a Bruker Avance IIIHD 500 instrument operating at 500, 125, and 470.4 MHz, respectively, or on a Varian Mercury Vx 400 operating at 400, 100, and 376.5 MHz, respectively. Chemical shifts are listed in parts per million (ppm) and were referenced using the residual nondeuterated solvent ^{1}H signal or the solvent ^{13}C resonance, or, for ^{19}F NMR, using an internal standard (trifluoroacetic acid, −76.55 ppm). Column chromatography was carried out using silica gel (60 Å, 40–63 μm, Sorbent) as the stationary phase. Mass spectra were measured on an Applied Biosystems 4700 Proteomics Analyzer using MALDI or a VG Instruments 70-SE using electron impact (EI) mode. UV–vis spectra were measured using a Cary 5000 UV–vis–NIR spectrophotometer. Fluorescence, phosphorescence, and emission transients were collected on a Jobin Yvon Fluorolog-3 equipped with a pulsed xenon lamp, photomultiplier tube (Horiba R928), and pulsed LED excitation source (NanoLED). Fluorescent lifetimes were fit using DAS6 decay analysis software. Solution and solid-state absolute PLQYs were determined on a Quantaurus-QY C11347 spectrometer. Spin-cast thin films were cast from chloroform onto quartz substrates at 500 rpm for 2 min, then dried under high vacuum. Electrochemical data were acquired using cyclic voltammetry in

0.1 M $^{n}Bu_4N^+PF_6^-$ in dry tetrahydrofuran for reductive scans under nitrogen, using a CH Instruments 620D potentiostat, a glassy carbon working electrode, a platinum wire auxiliary electrode, and, as a pseudo-reference electrode, a silver wire anodized in 1 M aqueous potassium chloride solution. The scan rate was 50 mV s^{-1}, and ferrocene was added as an internal reference. Thermogravimetric analysis was carried out using a PerkinElmer Pyris 1 TGA with a heating rate of 10 °C min^{-1}.

Scheme 1. Syntheses Described in the Experimental Section.

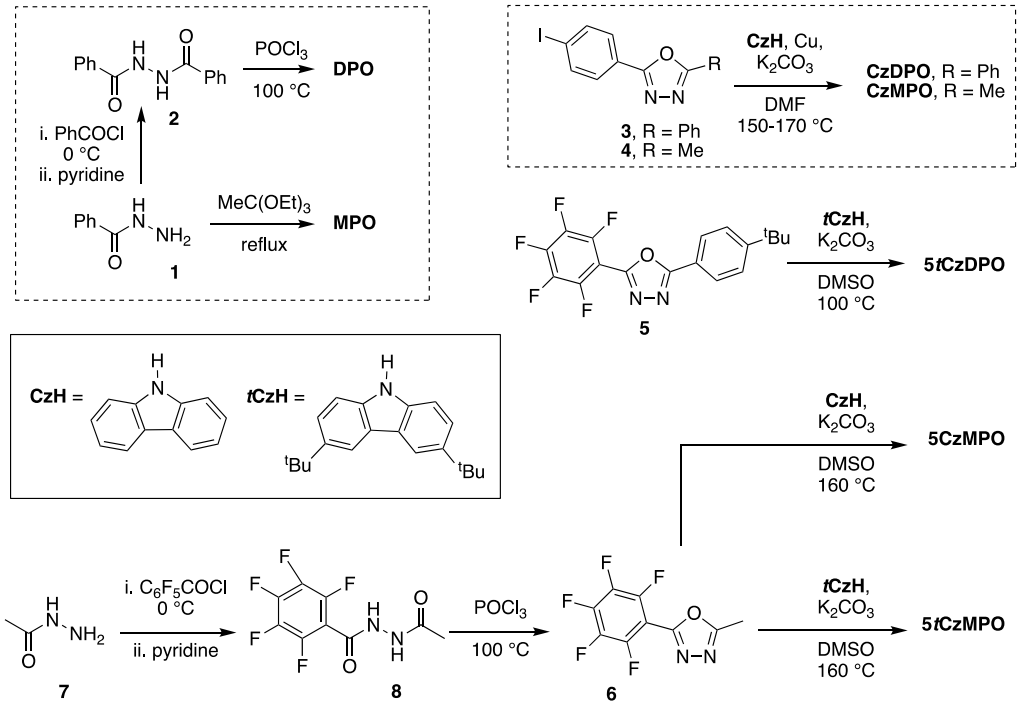

2,5-Diphenyl-1,3,4-oxadiazole (DPO). Benzohydrazide (**1**, 0.992 g, 7.29 mmol) was dissolved in dry THF (25 mL) in a dry round-bottomed flask under N_2 at 0 °C in an ice bath, to which benzoyl chloride (0.85 mL, 7.34 mmol) was added dropwise. After the benzoyl chloride was added, the reaction mixture was removed from the ice bath, allowed to warm to room temperature, and stirred overnight. Pyridine (2 mL) was added and the reaction mixture was further stirred for 30 min. Water (30 mL) was added to precipitate to white a white solid, which was collected via filtration. The product, *N'*-benzoylbenzohydrazide (**2**) was obtained as a white powder (1.39 g) and was used in the next step without further purification.

2 (1.39 g, 5.79 mmol) was suspended in $POCl_3$ (10 mL) in a round-bottomed flask and heated in an aluminum block at 100 °C and stirred for 6 h. After cooling to room temperature, the reaction mixture was poured over ice and the white precipitate was collected via filtration to yield the product (1.28 g, 80%). ^{1}H NMR (500 MHz, $CDCl_3$): δ 8.16-8.14 (m, 4H), 7.56-7.54 (m, 6H). $^{13}C\{^1H\}$ NMR (125 MHz, $CDCl_3$): δ 164.58, 131.71, 129.07, 126.93, 123.93. HRMS (EI, *m/z*) Calcd for $C_{14}H_{10}N_2O$ $[M]^+$, 222.0793; Found 222.0801. Anal. Calcd for $(C_{14}H_{10}N_2O)_6 \cdot H_2O$: C, 74.65; H, 4.62; N, 12.44. Found: C, 74.55; H, 4.84; N, 12.28.

2-Methyl-5-phenyl-1,3,4-oxadiazole (MPO). Benzohydrazide (**1**, 0.992 g, 7.29 mmol) was placed in a round-bottomed flask with a stir bar, which was evacuated and placed under a nitrogen atmosphere. Triethyl orthoacetate (5.0 mL, 27 mmol) was added and the reaction mixture was heated in an aluminum heat block to reflux and stirred for 24 h. After cooling, the excess triethyl orthoacetate was removed under reduced pressure, and the residue was purified via column chromatography (silica gel) using dichloromethane as the eluent, followed by 5% methanol in dichloromethane. The product was obtained as a white, crystalline powder (0.471 g, 40%). ^{1}H NMR (500 MHz, $CDCl_3$): δ 8.02 (d, J = 8.5 Hz, 2H); 7.52-7.47 (m, 3H); 2.61 (s, 3H). $^{13}C\{^1H\}$ NMR (125 MHz, $CDCl_3$): δ 164.85; 164.58; 131.49; 128.49; 128.67; 123.94; 11.07. These NMR data are consistent with reported spectra.[28]

2-(4-(9*H*-Carbazol-9-yl)phenyl)-5-phenyl-1,3,4-oxadiazole (CzDPO). To a solution of carbazole (**CzH**, 5.0 g, 30 mmol), 2-(4-iodophenyl)-5-phenyl-1,3,4-oxadiazole[29] (**3**, 5.0 g, 15 mmol), and Cu (3.0 g, 47 mol) in DMF (30 mL) in a round-bottomed flask was added K_2CO_3(10.0 g, 72.4 mmol) under nitrogen with stirring. The reaction mixture was heated in an aluminum heating block at 150 °C for 9 h. After cooling, the reaction mixture was filtered and the solid was washed with THF. The filtrate was concentrated under reduced pressure and water was added to the remaining DMF solution; a brown solid precipitated and was collected via filtration. The crude product was purified by column chromatography using dichloromethane as the eluent. The product was recrystallized from methanol/water and the white solid product was collected by filtration (4.8 g 86%). ^{1}H NMR (400 MHz, $CDCl_3$): δ 8.39 (d, J = 8.8 Hz, 2H), 8.21-8.15 (m, 4H), 7.79 (d, J = 8.8 Hz, 2H), 7.59-7.57 (m, 3H), 7.53-7.51 (m, 2H), 7.46 (t, J = 6.8 Hz, 2H), 7.33 (t, J = 6.8 Hz, 2H). $^{13}C\{^1H\}$ NMR (100 MHz, $CDCl_3$): δ 164.73, 163.96, 140.85, 140.20, 131.83, 129.11, 128.52, 127.17, 126.94, 126.18, 123.79, 123.75, 122.41, 120.55, 120.44, 109.66. NMR data are consistent with those previously reported.[18]

2-(4-(9*H*-Carbazol-9-yl)phenyl)-5-methyl-1,3,4-oxadiazole (CzMPO). To a solution of carbazole (**CzH**, 3.5 g, 21 mmol), 2-(4-iodophenyl)-5-methyl-1,3,4-oxadiazole (**4**, 5.0 g, 17.5 mmol),[30] and Cu (5.0 g, 80 mol) in DMF (50 mL) was added K_2CO_3 (10 g, 72 mmol) under nitrogen with stirring. The reaction mixture was heated in an aluminum heating block at 170 °C for 21 h. After cooling, the reaction mixture was filtered, and the solid residue was washed with THF. The filtrate was concentrated under reduced pressure and water was added to the remaining DMF solution. The brown precipitate was collected via filtration and washed with methanol. The solid was purified by column chromatography using dichloromethane/ethyl acetate (95:5) as the eluent. The product was recrystallized from dichloromethane/methanol and collected via filtration to yield the product as a white powder (4.9 g, 87%). ^{1}H NMR (400 MHz, $CDCl_3$): δ 8.27 (d, *J* = 8.8 Hz, 2H), 8.16 (d, *J* = 7.6 Hz, 2H), 7.74 (d, *J* = 8.8 Hz, 2H), 7.50-7.42 (m, 4H), 7.33 (t, *J* = 8.0 Hz, 2H), 2.67 (s, 3H). ^{13}C{^{1}H} NMR (100 MHz, $CDCl_3$): δ 164.26, 163.81, 140.68, 140.20, 128.31, 127.13, 126.15, 123.71, 122.49, 120.50, 120.41, 109.64, 11.16. HRMS (ESI, *m/z*): Calcd for $C_{21}H_{16}N_3O$, 326.1288 $[M]^+$; Found 326.1289. NMR data are consistent with those previously reported.[18]

2-(4-(*tert*-Butyl)phenyl)-5-(2,3,4,5,6-pentakis(3,6-di-tert-butyl-9*H*-carbazol-9-yl)phenyl)-1,3,4-oxadiazole (5*t*CzDPO). A solution of 3,6-di-*tert*-butylcarbazole (***t*CzH**, 1.9 g, 6.8 mmol), 2-(4-*(tert*-butyl)phenyl)-5-(perfluorophenyl)-1,3,4-oxadiazole[21] (**5**, 0.50 g, 1.4 mmol), and K_2CO_3 (2.0 g, 15 mmol) in DMSO (20 ml) was stirred at 50 °C for 24 h, and then at 100 °C for 26 h under nitrogen. After cooling to room temperature, water (100 mL) was added and a yellow solid was obtained. The solid product was collected by filtration, washed with water and dried on the filter. The crude product was purified by column chromatography (silica gel) using dichloromethane/hexane (4:6) as eluent. After removal of the solvent under reduced pressure, the product was recrystallized from dichloromethane/methanol and the yellow solid was collected by filtration. After drying under vacuum, the product was obtained as a yellow powder (1.8 g, 78%). ^{1}H NMR (400 MHz, $CDCl_3$): δ 7.51 (d, *J* = 1.6 Hz, 4H), 7.26 (d, *J* = 2.0 Hz, 4H), 7.23 (d, *J* = 2.0 Hz, 2H), 7.12 (d, *J* = 8.8 Hz, 2H), 6.96 (m, 14H), 6.78 (d, *J* = 8.8 Hz, 2H), 6.62 (m, 6H), 1.24 (s, 9H), 1.23 (s, 36H), 1.22 (s, 36H), 1.21 (s, 18H) ppm. ^{13}C{^{1}H} NMR (100 MHz, $CDCl_3$): δ 163.72, 157.78, 154.50, 142.64, 142.56, 142.48, 139.97, 138.51, 137.81, 137.54, 137.27, 137.09, 126.63, 126.37, 124.90, 124.17, 124.10, 124.00, 122.94, 122.00, 119.98, 115.73, 115.66, 114.85, 110.21, 110.09, 109.00, 34.36, 34.24, 31.79, 31.77, 31.74, 30.98 HRMS (MALDI, *m/*z): Calcd for $C_{118}H_{133}N_7O$ (M^+) 1664.0572; Found 1664.0618. Anal. Calcd for $C_{118}H_{133}N_7O$: C, 85.10; H, 8.05; N, 5.89. Found: C, 85.08; H, 8.05; N, 5.77.

2-Methyl-5-(perfluorophenyl)-1,3,4-oxadiazole (6). To a solution of acetohydrazide (**7**, 3.2 g, 43 mmol) in dry THF (100 mL) was slowly added 2,3,4,5,6-pentafluorobenzoyl chloride (10.0 g, 43.4 mmol) at 0 °C under nitrogen, during which addition a white solid appeared. After the addition was complete, the reaction was allowed to warm to room temperature. The reaction mixture was stirred for 6 h, and then pyridine (10 mL) was added and the mixture was stirred for an additional 20 min. Water (400 mL) was added to the reaction mixture. The resulting white solid was and collected by filtration. After drying under vacuum, the product, *N'*-acetyl-2,3,4,5,6-pentafluorobenzohydrazide (**8**), was obtained as white powder (9.2 g) andused for next step without any future purification.

8 (9.0 g, 34 mmol) was suspended in $POCl_3$ (75 mL) and heated to 100 °C with stirring (oil bath). During heating, the white solid starting materials dissolved and a clear reaction solution was obtained. The reaction was monitored by a thin layer chromatography (dichloromethane/ethyl acetate 9 : 1 as eluting solution). After 4 h, the reaction mixture was allowed to cool to room temperature and was carefully dropped into ice-cold water (700 mL). A white solid precipitated out and was collected by filtration and washed with water. Solvent was removed under reduced pressure and the crude product was purified by silica gel column chromatography, eluting with dichloromethane and ethyl acetate in 9 : 1 ratio. Solvent was again removed under reduced pressure and the white solid was recrystallized from methanol/water, and finally dried under vacuum. Pure product was obtained as a white solid (5.0 g, 48%, two steps). ^{1}H NMR (400 MHz, $CDCl_3$): δ 2.69 (s, 3H). ^{19}F NMR (376.5 MHz, $CDCl_3$, CF_3COOH): δ -135.82 (m, 2F), -147.37 (m, 1F), -159.60 (m, 2F).

2-Methyl-5-(2,3,4,5,6-penta(9*H*-carbazol-9-yl)phenyl)-1,3,4-oxadiazole (5CzMPO). 2-Methyl-5-(perfluorophenyl)-1,3,4-oxadiazole (**6**, 1.0 g, 4.0 mmol), carbazole (**CzH**, 3.6 g, 22 mmol), and potassium carbonate were dissolved in DMSO (20 mL) in a round-bottomed flask and stirred in an aluminum heating block at 70 °C for 1 h, 100 °C for 2 h, 120 °C for 14 h, and 160 °C for 4 h. After cooling to room temperature, water was added (150 mL) and the precipitate was collected via filtration and washed with water and then methanol. The crude product was purified via column chromatography using dichloromethane as the eluent. The product was recrystallized from dichloromethane/methanol, and filtration yielded the product as a pale-yellow powder (3.8 g, 97%). ^{1}H NMR (400 MHz, CDCl3): 7.67 (m, 4H), 7.33 (d, *J* = 7.6 Hz, 4H), 7.28 (d, *J* = 7.6 Hz, 2H), 7.18 (m, 10H), 6.97 (m, 8H), 6.78-6.57 (m, 12H), 1.54 (s, 3H). ^{13}C{^{1}H} NMR (100 MHz, $CDCl_3$): δ 163.29, 158.09, 139.57, 139.41, 138.22, 137.88, 137.82, 136.71, 127.32, 125.37, 124.36, 124.34, 123.69, 123.58, 123.57, 120.54, 120.31, 120.;22, 119.92, 119.85, 119.40, 110.67, 110.45, 109.51, 9.80. HRMS (MALDI), Calcd for $C_{69}H_{43}N_7O$: *m/z* = 985.3529 (M^+); Found: *m/z* = 985.3541. Anal. Calcd for $C_{69}H_{43}N_7O$: C, 84.04 %; H, 4.40 %; N, 9.94 %; Found: C, 84.05 %; H, 4.36 %; N, 9.93 %.

2-Methyl-5-(2,3,4,5-pentakis(3,6-di-*tert*-butyl-9*H*-carbazol-9-yl)phenyl)-1,3,4-oxadiazole (5*t*CzMPO). A solution of 2-methyl-5-(perfluorophenyl)-1,3,4-oxadiazole (**6**, 0.70 g, 2.8 mmol), 3,6-di-*tert*-butylcarbazole (***t*CzH**, 4.5 g, 16 mmol), and K_2CO_3 (10 g, 72 mmol) in DMSO (20 mL) was stirred under nitrogen at 120 °C for 15 h and then at 160 °C for 9 h. After cooling to room temperature, water (100 mL) was added and a pale-yellow precipitate was obtained. The solid was collected by filtration, washed with water and then methanol. The crude product was purified by column chromatography using dichloromethane/hexane (1:1) as eluent, followed by recrystallization from

dichloromethane/methanolto give a pale-yellow powder (3.5 g, 81%). ^{1}H NMR (400 MHz, $CDCl_3$): δ 7.56 (s, 4H), 7.24 (m, 6H), 7.01-6.85 (m, 14H), 6.59 (m, 6H), 1.60 (s, 3H), 1.29 (s, 36H), 1.22 (s, 36H), 1.18 (s, 18H). ^{13}C{^{1}H} NMR (100 MHz, $CDCl_3$): δ 163.09, 158.78, 142.72, 142.63, 142.41, 140.38, 138.11, 137.60, 137.29, 137.24, 136.67, 127.06, 124.22, 124.04, 123.84, 122.71, 121.90, 115.45, 115.37, 114.80, 110.28, 109.99, 109.13, 34.41, 34.22, 31.85, 31.80, 31.78, 31.74, 9.97. HRMS (MALDI, *m/z*): Calcd for $C_{109}H_{123}N_7O$, 1545.9789 (M^+); Found: 1545.9797. Anal. Calcd for $C_{109}H_{123}N_7O$: C, 84.62; H, 8.01; N, 6.34. Found: C, 84.35; H, 7.90; N, 6.25.

Computational Methodology. The electronic structure analyses were performed at the density functional theory (DFT) level using the screened range-separated hybrid (SRSH) functional[31 32]LC-ωhPBE and 6-31G (d, p) basis set. The range separation parameter, ω, was optimized in each case using a minimization procedure on the basis of the expression: $J(\omega) = [\varepsilon_{HOMO}(\omega) + IP(\omega)]^2 + [\varepsilon_{LUMO}(\omega) + EA(\omega)]^2$.[33] The dielectric constant of toluene was considered for the SRSH calculations.

The excited-state energies were estimated using the Tamm-Dancoff approximation (TDA)[34 35] within the time-dependent DFT. Natural Transition Orbitals (NTO) analyses[36] were performed to characterize the excited states. The spin-orbit coupling (SOC) values between the ground and excited states were estimated using the PySOC code[37] interfaced with TDA-TDDFT calculations. All DFT and TDA-TDDFT calculations were performed with the Gaussian 16 program.[38]

RESULTS AND DISCUSSION

Parent DPO and MPO Acceptors. We first consider some of the properties of the isolated **MPO** and **DPO** molecules. Specifically, the relative acceptor strength and the energy of the lowest lying triplet excited state of each compound are of critical importance in the design of efficient TADF fluorophores. As expected **MPO** is indeed a weaker electron acceptor than **DPO**. The electrochemical reductions are not reversible, but that for **MPO** is ca. 0.2 V more cathodic than that for **DPO** (Figure S1, Supporting Information). Furthermore, the phosphorescence spectrum of **MPO** is blue-shifted compared to that of DPO, with shifts of the maximum by 0.51 eV and of the onset by ca. 0.12 eV (Figure S2, Supporting Information), indicating a higher triplet energy for this acceptor.

Monocarbazolyl DPO and MPO Derivatives. We also compared two previously reported[18] simple donor-acceptor chromophores: **CzDPO** and **CzMPO**. As shown in Figure 1, both compounds have featureless steady-state PL spectra, attributed to fluorescence from CT-type S_1 states, and vibronically structured low-temperature delayed PL spectra, assigned to phosphorescence and consistent with T_1 states that have less CT character. The compounds show very similar spectral lineshapes to each other; as previously reported,[18] both fluorescence and phosphorescence spectra are blue shifted by ca. 0.12 eV for **CzMPO**, and, therefore both compounds have similar ΔE_{ST} values (ca. 0.73 eV using the high-energy onsets of room-temperature fluorescence in toluene and 77 K phosphorescence; previously estimated in a slightly different way as 0.78 and 0.76 eV[18]).

Figure 1. Spectra of **CzDPO** (open circles) and **CzMPO** (closed squares) in toluene. Black: absorption (black). Red: room-temperature steady-state PL attributed to fluorescence. Blue: PL collected at 77 K with a 500 μs delay between excitation and detection attributed to phosphorescence.

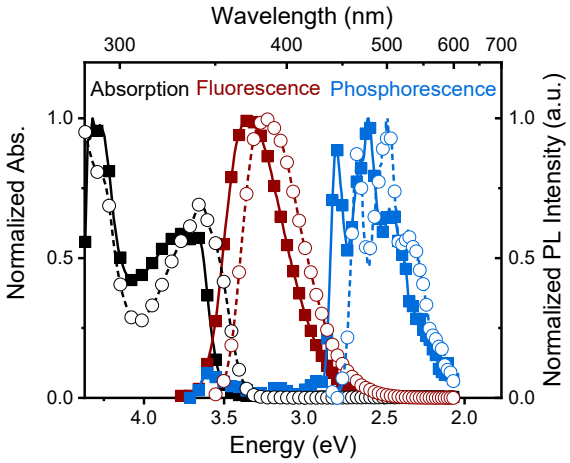

Quantum-chemical calculations at the SRSH-LC-whPBE/6-31G(d,p) level also indicate both S_1 and T_1 energies are 0.12-0.13 eV higher in **CzMPO** than in **CzDPO**, resulting in similar ΔE_{ST} values (0.79-0.80 eV) for the two compounds. Natural transition orbitals (NTOs) are consistent with inferences from spectra in indicating S_1 to have significant carbazole-to-oxadiazole CT character and T_1 to be more localized on the **DPO** or **MPO** moiety (see Figure 2 and Supporting Information, Figure S3). Interestingly, the electron NTO for the S_0-S_1 transition of **CzDPO** does not substantially extend onto the unsubstituted phenyl group. The calculations for each compound also suggest the presence of two carbazole-localized triplet states lying between T_1 and S_1 in energy (see Supporting Information, Figure S3).

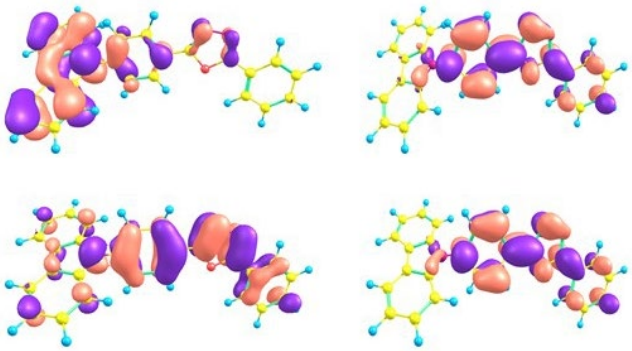

Figure 2. SRSH-LC-whPBE/6-31G(d,p) hole (left) and electron (right) NTOs for the S_0-S_1 (top) and S_0-T_1 (bottom) transitions of **CzDPO**.

Pentacarbazolylphenyl-oxadiazoles: synthesis and characterization. We have reported a high OLED external quantum efficiency (EQE) for a device using **5CzDPO** as the emitter. Here we examine the effects of replacing the DPO moiety with MPO, and also of replacing the carbazole-9-yl donors with 3,6-di-*tert*-butyl-9*H*-carbazol-9-yl (*t*Cz) groups, which are well known to be stronger donors based on electrochemical oxidation potentials (e.g., values of 1.23 and 1.38 V vs. Ag/AgCl have been reported for *N*-phenylcarbazole and 3,6-di-*tert*-butyl-*N*-phenylcarbazole,

respectively[39]) and on the energy of CT-type fluorescence in donor-acceptor compounds (e.g. in the comparison of 4-carbazol-9-yl and 4-(3,6-di-*tert*-butyl-carbazol-9-yl) derivatives of partially fluorinated diphenyl sulfones[26,40]). The compounds **5CzMPO**, **5*t*CzDPO**, and **5*t*CzMPO** were all synthesized through aromatic nucleophilic substitution reactions of the appropriate carbazole with 2-(4-*(tert*-butyl)phenyl)-5-(perfluorophenyl)-1,3,4-oxadiazole or 2-methyl-5-(perfluorophenyl)-1,3,4-oxadiazole (Scheme 1). We note that analogues of **5*t*CzDPO** in which the terminal phenyl ring is either unsubstituted or substituted with one or two CF_3 groups have recently been reported and were synthesized in a similar way.[26] All compounds also show good thermal stability with thermal gravimetric analysis indicating decomposition temperatures, defined as 5% weight loss, all in excess of 400 °C (Table 1).

Electrochemical data for the four compounds are shown in Table 1 (see also Supporting Information, Figure S5). The oxidation potentials are of limited use given the differences in reversibility between Cz and *t*Cz derivatives. However, the reduction potentials are consistent with the **MPO** moiety being a somewhat weaker acceptor than **DPO** (as also seen for isolated **DPO** and **MPO** as discussed above). The reduction potentials also depend on the donor; as in a recent report on analogues of **5CzDPO** and **5*t*CzDPO** differing only in lacking the ^{t}Bu substituent on the phenyl groups,[26] the *t*Cz derivatives are a little less easily reduced than their Cz counterparts, presumably due to the stronger π-donating and/or weaker inductively electron-withdrawing properties of the *t*Cz group.

Table 1. Oxidation and Reduction Potentials (vs. $FeCp_2^{+/0}$) and Decomposition Temperatures of Pentacarbazolylphenyl-Oxadiazole Derivatives.

	E_{ox}[a] / V	E_{red}[b] / V	T_d[c] / °C
5CzDPO[c]	+1.00	–2.19	478
5*t*CzDPO	+0.78	–2.28	440
5CzMPO	+1.00	–2.26	487
5*t*CzMPO	+0.78	–2.35	417

[a] $E_{pa}^{+/0}$ (Cz compounds) or $E_{1/2}^{+/0}$ (*t*Cz derivatives) in CH_2Cl_2 / 0.1 M Bu_4NPF_6. [b] $E_{1/2}^{0/-}$ in THF / 0.1 M Bu_4NPF_6. [c] 5% weight loss. [d] From ref. 22.

Pentacarbazolylphenyl-Oxadiazoles: Solution Spectra. Optical data were acquired for all four pentacarbazolyl species in toluene (Figure 3, Table 2, and Supporting Information, Figure S6). The room-temperature steady-state PL spectra of the **MPO**-based compounds are blue-shifted relative to those of their **DPO** counterparts, as is seen for **CzDPO** and **CzMPO** (Figure 1). The S_1 energies, estimated from the onset of these spectra, are 0.05-0.06 eV higher for compounds containing the **MPO** acceptor than for their **DPO** counterparts. As expected, the S_1 energy decreases (by 0.08-0.09 eV) when the stronger *t*Cz donors are used in place of Cz. These observations, along with the broad, structureless lineshape of the fluorescent emission and the sensitivity of the Stokes shift to the solvent polarity Supporting Information, Figure S7) are consistent with the S_1 states having significant CT character.

Table 2. Experimental Photophysical Properties for Pentacarbazolylphenyl-Oxadiazole Derivatives in Dilute Toluene Solution along with Parameters from SRSH-LC-whPBE/6-31G(d,p) TDA-TDDFT Calculations in Italics.

	Absorption	Fluorescence[a]		Phosphorescence[b]						
	λ_{max} / nm	λ_{max} / nm	E_{S1} / eV	λ_{max} / nm	E_{T1} / eV	ΔE_{ST}[c] / eV	Φ_{PL} (air; N_2)[d]	τ_{PL}[e] / ns; µs	k_{RISC} / 10^5 s^{-1}	SO[f] / cm^{-1}
5CzDPO[g]	291, 333	482	2.93, 3.07	459	2.81, *2.86*	0.12, *0.20*	0.03; 0.13	2.9; 62.8	5.3	*0.748*
5*t*CzDPO	297, 342	496	2.84, *2.94*	488	2.83, *2.77*	0.01, *0.16*	0.05; 0.20	2.8; 30.4	6.6	*0.633*
5CzMPO	285, 333	466	2.98, *3.15*	416	2.86, *2.92*	0.12, *0.23*	0.08; 0.21	2.8; 11.0	11	*0.921*
5*t*CzMPO	340	485	2.90, *3.03*	448	2.87, *2.83*	0.03, *0.19*	0.08; 0.30	3.1; 8.0	16	*0.885*

[a] Steady-state PL at room temperature; experimental E_{S1} energies from onset. [b] PL acquired at 77 K with a 500 µs delay; experimental E_{T1} from onset. [c] $\Delta E_{ST} = E_{S1} - E_{T1}$. [d] PL quantum yield in aerated and N_2-sparged solution. [e] Lifetimes of prompt and delayed PL. [f] S_1-T_1 spin-orbit coupling. [g] Data from ref. 21.

The T_1 energies estimated from the onset of the delayed PL spectra at 77 K, are sensitive to the acceptor moiety but not the donor, being ca. 0.05 eV higher in the **MPO** derivatives than in their **DPO** analogues. Taken together with the trends in S_1 energies noted above, the estimated ΔE_{ST} values are approximately the same for **DPO** and **MPO** derivatives with the same substitution (Table 2). When the donor is changed from Cz to *t*Cz, the T_1 energy estimated from the onset of the 77 K delayed PL is almost unchanged. However, these delayed emission spectra differ in their vibronic structure and the delayed PL *maxima* of the *t*Cz derivatives are significantly red-shifted from those of their Cz analogues. The apparent ΔE_{ST} values of the *t*Cz derivatives are ca. 0.02 eV, ca. 0.1 eV lower than those of their Cz containing counterparts. Similar differences between Cz and *t*Cz derivatives have been seen in analogues of **5CzDPO** and **5*t*CzDPO** lacking ^{t}Bu substituents on the phenyl group.[26] Thus, most of these spectroscopic properties are qualitatively consistent with what is seen for **CzDPO** and **CzMPO** and with our original hypothesis. However, the changes in delayed PL spectral profile between Cz and *t*Cz derivatives hint against a simplistic interpretation in which all the T_1 states are localized on the **DPO** or **MPO** moieties.

Transient photoluminescence of each compound displayed a two-component decay when collected in nitrogen sparged solution (Figure 3, insets), with the long-lifetime component disappearing in the presence of oxygen, as expected if the delayed component represents TADF. Consistent with this observation, each compound also showed a significant increase in PLQY when sparged with nitrogen. Values of k_{RISC} were estimated for each compound,[41] and are shown in Table 1 along with the prompt and delayed emission

lifetimes. The **MPO**-based compounds exhibited k_{RISC} approximately twice those of their **DPO** analogues, despite comparable estimated ΔE_{ST} values.

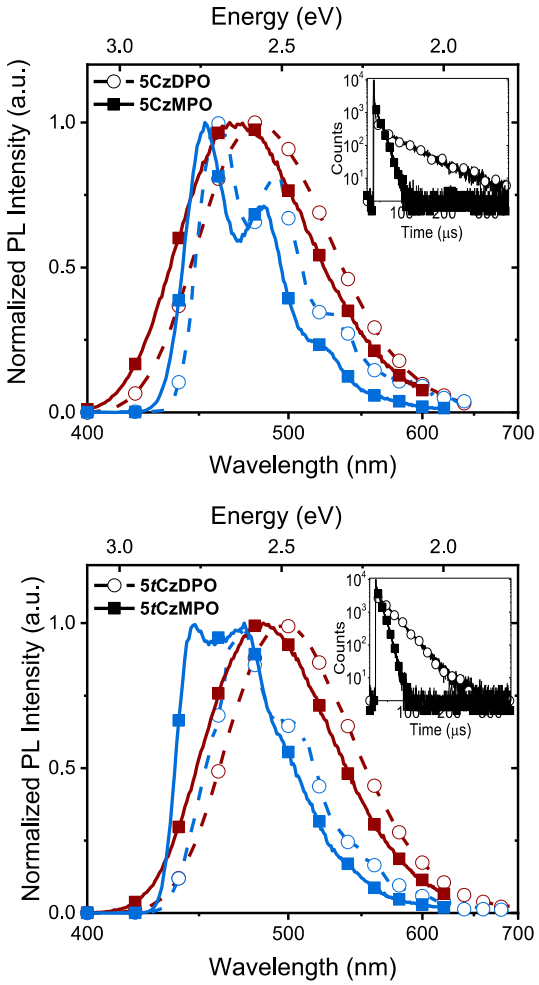

Figure 3. Steady-state room-temperature PL, attributed to fluorescence (red) and PL at 77 K collected with a 500 μs delay between excitation and detection, attributed to phosphorescence (blue) of pentacarbazolylphenyl-oxadiazoles with Cz (top) and *t*Cz donors (bottom), all recorded in dilute toluene solution. The insets show room-temperature transient photoluminescence in nitrogen sparged toluene solution.

Pentacarbazolylphenyl-Oxadiazoles: TD-DFT. Quantum-chemical calculations (SRSH-LC-whPBE/6-31G(d,p)) qualitatively reproduce many of the trends discussed above (see Table 2 and Figures S8-11 in the Supporting Information). In particular, they afford small ΔE_{ST} values (≤ 0.2 eV for **5CzDPO**, **5*t*CzDPO**, and **5*t*CzMPO**; 0.23 eV for the case of **5CzMPO**). The ΔE_{ST} values are smaller for the Cz derivatives that their *t*Cz analogues, and indicate that **MPO** derivatives have higher energy S_1 and T_1 states than their **DPO** counterparts. Contrary to the inferences from the delayed PL onset, but consistent with delayed PL maxima, the calculated T_1 energies are somewhat lower in energy for the *t*Cz compounds than their Cz counterparts.

As expected, as calculated for the monocarbazolyl species (above), and as previously calculated for **5CzDPO** at the MPW1B95/6-31G(d,p) level, the S_0-S_1 NTOs calculated for the pentasubstituted compounds have considerable carbazole-to-oxadiazole CT character. In each case the electron NTOs are similar to those for **CzDPO** and **CzMPO**, i.e., predominantly localized on the oxadiazole itself and the carbazole-substituted benzene ring. The presence of multiple carbazole donors leads to multiple CT-type singlet states that closely spaced in energy.

In contrast to our original assumptions, and to the calculated S_0–T_1 NTOs for **CzDPO** and **CzMPO**, the calculated S_0–T_1 NTOs for the pentacarbazolyl compounds are not purely localized on the DPO/MPO moieties, but have some CT character involving carbazole donors, and thus somewhat resembling the corresponding S_0–S_1 NTOs. However, the hole NTOs – shown in Figure 4 for the example of **5CzMPO** and in the Supporting Information, Figures S8, S10, and S11 for the other compounds – have carbazole character, but also much larger coefficients on the bridging phenyl ring than those for S_0–S_1, while the electron NTOs are similar to those for S_0–S_1. As in the case of the singlet transitions, several such low-lying states are found. We note that the NTOs are similar to LC-whPBE/6-31G(d,p) S_0–T_1 NTOs previsouly reported for **5CzDPO**.[21]

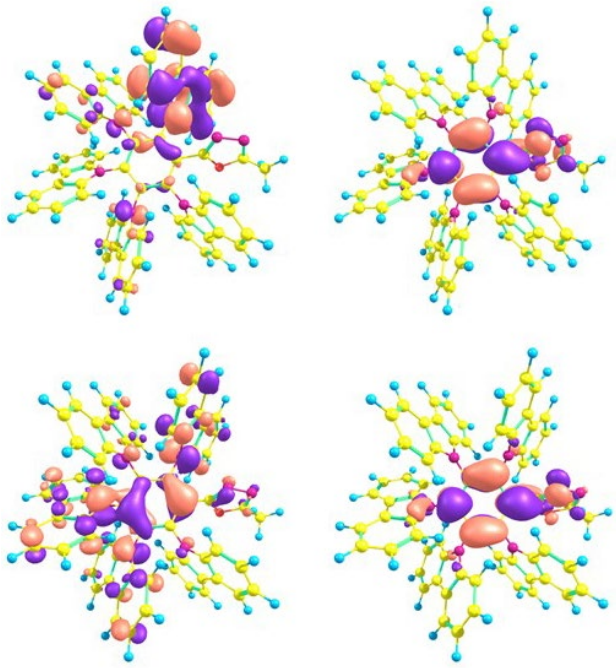

Figure 4. SRSH-LC-whPBE/6-31G(d,p) hole (left) and electron (right) NTOs for the S_0-S_1 (top) and S_0-T_1 (bottom) transitions of **5CzMPO**.

Spin-orbit couplings were also evaluated; S_0-T_1 couplings were found to be somewhat larger for the two **MPO** derivatives than for their **DPO** counterparts, consistent with the increased RISC rates estimated for the former compounds. The couplings are smaller for the *t*Cz compounds than their Cz counterparts: the competing effects of smaller spin-orbit coupling and smaller ΔE_{ST} presumably lead to each *t*Cz derivative exhibiting a similar experimentally estimated value of k_{RISC} as its Cz analogue.

Pentacarbazolylphenyl-Oxadiazoles: Solid-State Spectra. Thin films were spin-cast from chloroform solution (500 rpm, 60 s) in which the fluorophore was doped into bis[2-(diphenylphosphoryl)phenyl]ether (DPEPO, see

Figure 5 for structure) at 12.5 wt %. The PL maxima (Table 3) are blue-shifted from, but follow the same trend as, those observed in dilute toluene solution in that the MPO derivatives exhibit slightly higher energy emissions than their DPO counterparts. For each compound, both the PLQY and the delayed fluorescent lifetime (τ_{DF}) are greatly increased when compared to those in toluene solution, consistent with reduced nonradiative decay rates when dispersed in a film rather than in dilute solution.

Table 3. PL Properties of Pentacarbazolyl DPO and MPO Derivatives as 12.5 wt% Blends with DPEPO.

	λ_{max} / nm	Φ_{PL}[a]	CIE (x,y)	τ_{DF} / μs
5CzDPO	467	0.53	0.16, 0.22	215
5tCzDPO	474	0.79	0.17, 0.29	71
5CzMPO	462	0.51	0.16, 0.18	105
5tCzMPO	466	0.81	0.16, 0.20	69

[a]Under nitrogen flow.

As in solution, the solid-state PL quantum yields of the two *t*Cz-containing compounds higher than those of their respective Cz analogues, while the delayed fluorescent lifetimes are shorter, consistent with the contribution of smaller ΔE_{ST} values to k_{RISC}. The delayed fluorescence lifetimes are also slightly decreased in the MPO containing compounds when compared to their DPO containing analogues, as is also seen in solution.

Pentacarbazolylphenyl-Oxadiazoles: Electroluminescence. Each compound was evaluated as an emitter doped into the emissive layer of an OLED. The device structure was adopted from our recent work on blue-green TADF OLEDs[42] without optimization and is shown below in Figure 5. The electroluminescence (EL) spectra are somewhat red-shifted relative to the corresponding solid-state PL spectra, resulting in more greenish emission. Moreover, the detailed compound-to-compound variation in EL spectra does not follow those in the solution or solid-state PL spectra, as we have also observed in some of our previous studies.[21] In particular, all four emitters exhibit similar EL maxima but, due to the EL lineshape differences, somewhat different chromaticities

Table 4. Performance of OLEDs Using Pentacarbazolyl DPO and MPO Emitters

		%EQE		current efficacy / cd A^{-1}		power efficacy / lm W^{-1}		
emitter	V_{on}[a] / V	10 cd m^{-2}	1000 cd m^{-2}	10 cd m^{-2}	1000 cd m^{-2}	10 cd m^{-2}	1000 cd m^{-2}	CIE(x,y)[b]
5CzDPO	4.1	24	9.3	46	18	35	6.5	0.17, 0.32
5*t*CzDPO	3.9	29	13	62	29	46	10	0.18, 0.36
5CzMPO	4.1	15	7.2	30	14	21	3.7	0.21, 0.32
5*t*CzMPO	4.1	23	16	47	34	39	12	0.18, 0.34

[a]Turn-on voltage, defined as that required to obtain 10 cd m^{-2}. [b]From EL spectra obtained under a bias of 5V.

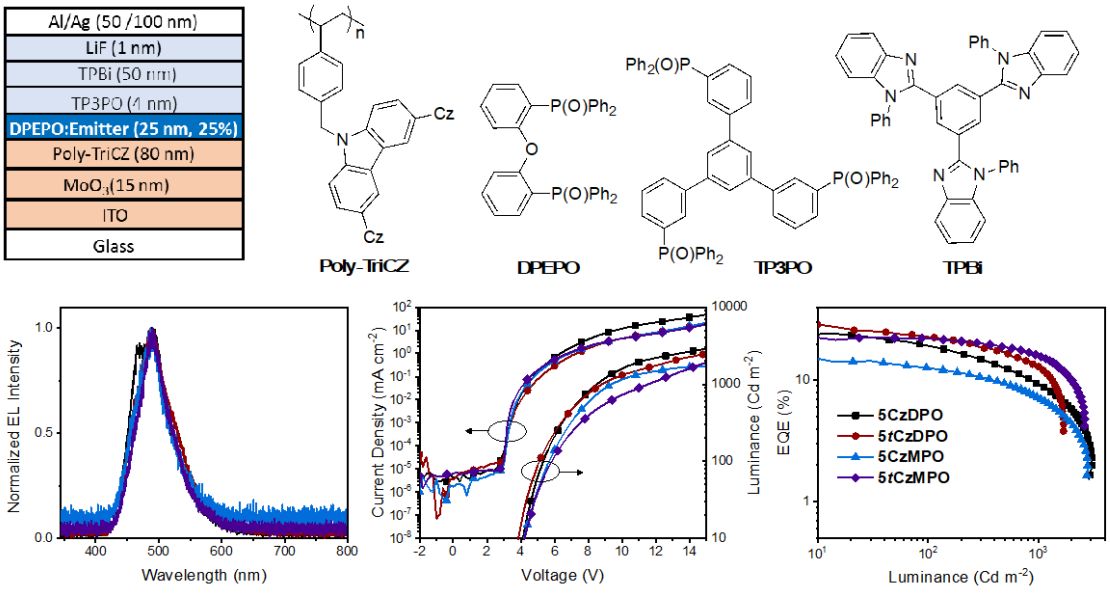

Figure 5. Top: OLED structure used to examine the EL behavior of pentacarbazolylphenyl-oxadiazole emitters, along with the chemical structures of the hole-transport, host, and electron-transport materials used. Bottom: EL spectra (left), current-voltage-luminescence characteristics (center), and EQE (right) of the devices.

The higher PLQY of the *t*Cz-containing compounds relative to the Cz-containing compounds, earlier attributed to the larger contribution of delayed fluorescence to the total PLQY, may be responsible for the higher maximum external quantum efficiency (EQE_{max}) value seen for each *t*Cz emitter than for its Cz analogue.

The MPO devices exhibit less pronounced roll off in EQE than their DPO analogues as the driving voltage and

brightness is increased. At a luminance of 1000 cd m^{-2} the device with **5CzMPO** retains 48% of its EQE at 10 cd m^{-2}, while **CzDPO** retains 39% of its EQE. Similarly, at a luminance of 1000 cd m^{-2} the EQE of the **5*t*CzMPO** is 70% of that at 10 cd m^{-2}, while that of ***5t*CzDPO** is 42% of that at 10 cd m^{-2}. Indeed, the **5*t*CzMPO** device is the most efficient of all the four devices at a luminance of 1000 cd m^{-2}. EQE roll-off in EL devices is generally attributed to processes such as triplet-triplet and carrier-triplet annihilation becoming more significant at higher triplet exciton concentrations resulting from higher current densities.[43] The reduced roll-off seen for the MPO derivatives may be due to the effects of the increased RISC rates, and consequently shorter values of τ_{DFn} observed for the MPO derivatives, in reducing triplet exciton concentrations at high current densities. However, the effects of the different emitters on charge-transport, and thus the location of the recombination zone, may also play a role.

CONCLUSIONS

Pentacarbazolyl derivatives of MPO exhibit higher T_1 and S_1 energies than, and similar ΔE_{ST} values to, their DPO analogues. Although these results may be rationalized based on simple pictures of DPO/MPO-localized triplet excitations and CT singlet states, as in the case of simpler monocarbazolyl derivatives, TD-DFT calculations reveal a more complex description. The solution spectroscopic trends suggest that use of MPO in place of DPO in donor-acceptor architectures may be a useful approach to obtaining efficient blue-emitting OLEDs. In the present study, the blue shift of emission seen in solution PL data is not preserved in the OLEDs fabricated; more work is needed to understand the generality and cause of this observation. However, the devices incorporating the MPO emitters do exhibit reduced efficiency roll-off at high current densities relative to their DPO counterparts; this correlates with shorter delayed fluorescence lifetimes and may be a result of higher RISC rates, which in turn may be due to the higher spin-orbit couplings between S_1 and T_1 states seen in quantum-chemical calculations for these fluorophores. Use of other MPO-based TADF fluorophores in place of their DPO counterparts may therefore be advantageous in OLEDs, both in terms of tuning emission color and reducing efficiency roll off.

ASSOCIATED CONTENT

Supporting Information

The Supporting Information is available free of charge on the ACS Publications website.

Additional electrochemical, spectroscopic, and computational data (PDF)

AUTHOR INFORMATION

Corresponding Authors

* kippelen@gatech.edu; stephen.barlow@colorado.edu; seth.marder@colorado.edu.

Author Contributions

The manuscript was written through contributions of all authors. / All authors have given approval to the final version of the manuscript.

ACKNOWLEDGMENT

This material is based upon work supported in part by the Samsung Advanced Institute of Technology (SAIT) GRO Program, and upon work supported by the U.S. Department of Energy's Office of Energy Efficiency and Renewable Energy (EERE) under the Solid-State Lighting Program (Award Number DE-EE0008205). The work at Clark Atlanta University was supported under NSF Award HRD-1955299. The Georgia Tech Hive cluster and XSEDE clusters (under Research Allocation Award: TG-DMR200030 and Start-up Allocation Award: TG-CHE200101) are acknowledged for computational resources and technical support.

REFERENCES

(1) Uoyama, H.; Goushi, K.; Shizu, K.; Nomura, H.; Adachi, C., Highly Efficient Organic Light-Emitting Diodes from Delayed Fluorescence. *Nature* **2012,** *492*, 234-238.

(2) Liu, Y.; Li, C.; Ren, Z.; Yan, S.; Bryce, M. R., All-Organic Thermally Activated Delayed Fluorescence Materials for Organic Light-Emitting Diodes. *Nat. Rev. Mater.* **2018,** *3*, 18020.

(3) Wong, M. Y.; Zysman-Colman, E., Purely Organic Thermally Activated Delayed Fluorescence Materials for Organic Light-Emitting Diodes. *Adv. Mater.* **2017,** *29*, 1605444.

(4) Xie, F.-M.; Zhou, J.-X.; Li, Y.-Q.; Tang, J.-X., Effects of the Relative Position and Number of Donors and Acceptors on the Properties of TADF Materials. *J. Mater. Chem. C* **2020,** *8*, 9476-9494.

(5) Zhang, M.; Zheng, C.-J.; Lin, H.; Tao, S.-L., Thermally Activated Delayed Fluorescence Exciplex Emitters for High-Performance Organic Light-Emitting Diodes. *Mater. Horiz.* **2021,** *8*, 401-425.

(6) Samanta, P. K.; Kim, D.; Coropceanu, V.; Brédas, J.-L., Up-Conversion Intersystem Crossing Rates in Organic Emitters for Thermally Activated Delayed Fluorescence: Impact of the Nature of Singlet Vs Triplet Excited States. *J. Am. Chem. Soc.* **2017,** *139*, 4042-4051.

(7) Gibson., G.; Monkman, A. P.; Pendfold, T. J.., The Importance of Vibronic Coupling for Efficient Reverse Intersystem Crossing in Thermally Activated Delayed Fluorescence Molecules. *ChemPhysChem* **2016,** *17*, 2956-2961.

(8) Adachi, C.; Tsutsui, T.; Saito, S., Blue Light-Emitting Organic Electroluminescent Devices. *Appl. Phys. Lett.* **1990,** *56*, 799-801.

(9) Adachi, C.; Tsutsui, T.; Saito, S., Confinement of Charge Carriers and Molecular Excitons within 5-nm-Thick Emitter Layer in Organic Electroluminescent Devices with a Double Heterostructure. *Appl. Phys. Lett.* **1990,** *57*, 531-533.

(10) Kulkarni, A. P.; Tonzola, C. J.; Babel, A.; Jenekhe, S. A., Electron Transport Materials for Organic Light-Emitting Diodes. *Chem. Mater.* **2004,** *16*, 4556-4573.

(11) Hughes, G.; Bryce, M. R., Electron-Transporting Materials for Organic Electroluminescent and Electrophosphorescent Devices. *J. Mater. Chem.* **2005,** *15*, 94-107.

(12) Leung, M.-k.; Yang, C.-C.; Lee, J.-H.; Tsai, H.-H.; Lin, C.-F.; Huang, C.-Y.; Su, Y. O.; Chiu, C.-F., Unusual Electrochemical and Photophysical Behavior of 2,2'-Bis(1,3,4-Oxadiazol-2-yl)Biphenyls, Effective Electron Transport Hosts for Phosphorescent Organic Light Emitting Diodes. *Org. Lett.* **2007,** *9*, 235-238.

(13) Tao, Y.; Wang, Q.; Yang, C.; Wang, Q.; Zhang, Z.; Zou, T.; Qin, J.; Ma, D., A Simple Carbazole/Oxadiazole Hybrid Molecule: An Excellent Bipolar Host for Green and Red Phosphorescent Oleds. *Angew. Chem., Int. Ed.* **2008,** *47*, 8104-8107.

(14) Tao, Y.; Wang, Q.; Yang, C.; Zhong, C.; Zhang, K.; Qin, J.; Ma, D., Tuning the Optoelectronic Properties of Carbazole/Oxadiazole Hybrids through Linkage Modes: Hosts for Highly Efficient Green Electrophosphorescence. *Adv. Funct. Mater* **2010,** *20*, 304-311.

(15) Zhang, Y.; Zuniga, C.; Kim, S.-J.; Cai, D.; Barlow, S.; Salman, S.; Coropceanu, V.; Brédas, J.-L.; Kippelen, B.; Marder, S., Polymers with Carbazole-Oxadiazole Side Chains as Ambipolar Hosts for Phosphorescent Light-Emitting Diodes. *Chem. Mater.* **2011,** *23*, 4002–4015.

(16) Zhang, Y.; Haske, W.; Cai, D.; Barlow, S.; Kippelen, B.; Marder, S. R., Efficient Blue-Emitting Electrophosphorescent Organic Light-Emitting Diodes Using 2-(3,5-Di(Carbazol-9-yl)-Phenyl)-5-Phenyl-1,3,4-Oxadiazole as an Ambipolar Host,. *RSC Adv.* **2013,** *3*, 23514–23520

(17) Tang, C.; Chen, Y.; Wang, F.; Jiang, T.; Hu, J.; Cao, X.; Zhang, L.; Zhang, X., Effect of Methyl-Substitution on Carbazole /Oxadiazole Donor-Acceptor (D-A) Type Host Materials for Efficient Solution-Processed Green Organic Light-Emitting Diodes. *Tetrahedron* **2020,** *76*, 131030.

(18) Zheng, Y.; Batsanov, A. S.; Jankus, V.; Dias, F. B.; Bryce, M. R.; Monkman, A. P., Bipolar Molecules with High Triplet Energies: Synthesis, Photophysical, and Structural Properties. *J. Org. Chem.* **2011,** *76*, 8300-8310.

(19) Wong, M. Y.; Krotkus, S.; Copley, G.; Li, W.; Murawski, C.; Hall, D.; Hedley, G. J.; Jaricot, M.; Cordes, D. B.; Slawin, A. M. Z.; Olivier, Y.; Beljonne, D.; Muccioli, L.; Moral, M.; Sancho-Garcia, J.-C.; Gather, M. C.; Samuel, I. D. W.; Zysman-Colman, E., Deep-Blue Oxadiazole-Containing Thermally Activated Delayed Fluorescence Emitters for Organic Light-Emitting Diodes. *ACS Appl. Mater. Interf.* **2018,** *10*, 33360-33372.

(20) Zhang, D.; Cao, X.; Wu, Q.; Zhang, M.; Sun, N.; Zhang, X.; Tao, Y., Purely Organic Materials for Extremely Simple All-TADF White Oleds: A New Carbazole/Oxadiazole Hybrid Material as a Dual-Role Non-Doped Light Blue Emitter and Highly Efficient Orange Host. *J. Mater. Chem. C* **2018,** *6*, 3675-3682.

(21) Cooper, M. W.; Zhang, X.; Zhang, Y.; Jeon, S. O.; Lee, H.; Kim, S.; Fuentes-Hernandez, C.; Barlow, S.; Kippelen, B.; Marder, S. R., Effect of the Number and Substitution Pattern of Carbazole Donors on the Singlet and Triplet State Energies in a Series of Carbazole-Oxadiazole Derivatives Exhibiting Thermally Activated Delayed Fluorescence. *Chem. Mater.* **2018,** *30*, 6389-6399.

(22) Cooper, M. W.; Zhang, X.; Zhang, Y.; Fuentes-Hernandez, C.; Barlow, S.; Kippelen, B.; Marder, S. R., Control of Singlet Emission Energy in a Diphenyloxadiazole Containing Fluorophore Leading to Thermally Activated Delayed Fluorescence. *ACS Omega* **2018,** *3*, 14918-14923.

(23) Li, Z.; Li, W.; Keum, C.; Archer, E.; Zhao, B.; Slawin, A. M. Z.; Huang, W.; Gather, M. C.; Samuel, I. D. W.; Zysman-Colman, E., 1,3,4-Oxadiazole-Based Deep Blue Thermally Activated Delayed Fluorescence Emitters for Organic Light Emitting Diodes. *J. Phys. Chem. C* **2019,** *123*, 24772–24785.

(24) Abroshan, H.; Zhang, Y.; Zhang, X.; Fuentes-Hernandez, C.; Barlow, S.; Coropceanu, V.; Marder, S. R.; Kippelen, B.; Brédas, J.-L., Thermally Activated Delayed Fluorescence Sensitization for Highly Efficient Blue Fluorescent Emitters. *Adv. Funct. Mater.* **2020,** *30*, 2005898.

(25) Mayder, D. M.; Tonge, C. M.; Hudson, Z. M., Thermally Activated Delayed Fluorescence in 1,3,4-Oxadiazoles with π-Extended Donors. *J. Org. Chem.* **2020,** *85*, 11094-11103.

(26) Hu, D.; Zhu, M.; Shi, C.; Yuan, W.; Sun, N.; Huang, B.; Tao, Y., Manipulating Peripheral Non-Conjugated Substituents in Carbazole/Oxadiazole Hybrid TADF Emitters Towards High-Efficiency Oleds. *J. Mater. Chem. C* **2021,** *9*, 13384-13391.

(27) Wex, B.; Kaafarani, B. R., Perspective on Carbazole-Based Organic Compounds as Emitters and Hosts in TADF Applications. *J. Mater. Chem. C* **2017,** *5*, 8622-8653.

(28) Pouliot, M.-F.; Angers, L.; Hamel, J.-D.; Paquin, J.-F., Synthesis of 1,3,4-Oxadiazoles from 1,2-Diacylhydrazines Using $[Et_2NSF_2]BF_4$ as a Practical Cyclodehydration Agent. *Organic & Biomolecular Chemistry* **2012,** *10*, 988-993.

(29) Gierczyk, B.; Zalas, M.; Kazmierczak, M.; Grajewski, J.; Pankiewicz, R.; Wyrzykiewicz, B., ^{17}O Nmr Studies of Substituted 1, 3,4-Oxadiazoles. *Magn. Res. Chem.* **2011,** *49*, 648-654.

(30) Angell, R. M.; Bamborough, P.; Baldwin, I. R.; Li-Kwai-Cheung, A.-M.; Longstaff, T.; Merrick, S. J.; Smith, K. J.; Swanson, S.; Walker, A. L., Preparation of Heteroaryl Substituted Biphenyl Derivatives as P38 Kinase Inhibitors. *PCT Int. Appl. WO 2001-US47724* **2003**.

(31) Refaely-Abramson, S.; Sharifzadeh, S.; Jain, M.; Baer, R.; Neaton, J. B.; Kronik, L., Gap Renormalization of Molecular Crystals from Density-Functional Theory. *Phys. Rev. B* **2013,** *88*, 081204.

(32) Zheng, Z.; Egger, D. A.; Brédas, J.-L.; Kronik, L.; Coropceanu, V., Effect of Solid-State Polarization on Charge-Transfer Excitations and Transport Levels at Organic Interfaces from a Screened Range-Separated Hybrid Functional. *J. Phys. Chem. Lett.* **2017,** *8*, 3277–3283.

(33) Sun, H.; Zhong, C.; Brédas, J.-L., Reliable Prediction with Tuned Range-Separated Functionals of the Singlet-Triplet Gap in Organic Emitters for Thermally Activated Delayed Fluorescence. *J. Chem. Theory Comput.* **2015**, 10.1021/acs.jctc.5b00431, 3851-3858.

(34) Hirata, S.; Head-Gordon, M., Time-Dependent Density Functional Theory within the Tamm-Dancoff Approximation. *Chem. Phys. Lett.* **1999,** *314*, 291-299.

(35) Sears, J. S.; Koerzdoerfer, T.; Zhang, C.-R.; Brédas, J.-L., Orbital Instabilities and Triplet States from Time-Dependent Density Functional Theory and Long-Range Corrected Functionals. *J. Chem. Phys.* **2011,** *135*, 151103.

(36) Martin, R. L., Natural Transition Orbitals. *J. Chem. Phys.* **2003,** *118*, 4775.

(37) Gao, X.; Bai, S.; Fazzi, D.; Niehaus, T.; Barbatti, M.; Thiel, W., Evaluation of Spin-Orbit Couplings with Linear-Response Time-Dependent Density Functional Methods. *J. Chem. Theory Comput.* **2017,** *13*, 515-524.

(38) Frisch, M. J.; Trucks, G. W.; Schlegel, H. B.; Scuseria, G. E.; Robb, M. A.; Cheeseman, J. R.; Scalmani, G.; Barone, V.; Petersson, G. A.; Nakatsuji, H.; X. Li, M. C.; Marenich, A. V.; Bloino, J.; Janesko, B. G.; Gomperts, R.; Mennucci, B.; Hratchian, H. P.; Ortiz, J. V.; Izmaylov, A. F.; Sonnenberg, J. L.; Williams-Young, D.; Ding, F.; Lipparini, F.; Egidi, F.; Goings, J.; Peng, B.; Petrone, A.; Henderson, T.; Ranasinghe, D.; Zakrzewski, V. G.; Gao, J.; Rega, N.; Zheng, G.; Liang, W.; Hada, M.; Ehara, M.; Toyota, K.; Fukuda, R.; Hasegawa, J.; Ishida, M.; Nakajima, T.; Honda, Y.; Kitao, O.; Nakai, H.; Vreven, T.; Throssell, K.; Montgomery, J. A.; Peralta, J. E.; Ogliaro, F.; Bearpark, M. J.; Heyd, J. J.; Brothers, E. N.; Kudin, K. N.; Staroverov, V. N.; Keith, T. A.; Kobayashi, R.; Normand, J.; Raghavachari, K.; Rendell, A. P.; Burant, J. C.; Iyengar, S. S.; Tomasi, J.; Cossi, M.; Millam, J. M.; Klene, M.; Adamo, C.; Cammi, R.; Ochterski, J. W.; Martin, R. L.; Morokuma, K.; Farkas, O.; Foresman, J. B.; Fox, D. J. *Gaussian 16 Rev. C.01*, Gaussian Inc.: Wallingford, CT, 2016.

(39) Chiu, S.-K.; Chung, Y.-C.; Liou, G.-S.; Su, Y. O., Electrochemical and Spectral Characterizations of 9-Phenylcarbazoles. *J. Chin. Chem. Soc.* **2012,** *59*, 331-337.

(40) Drummond, B. H.; Aizawa, N.; Zhang, Y.; Myers, W. K.; Xiong, Y.; Cooper, M. W.; Barlow, S.; Gu, Q.; Weiss, L. R.; Gillett, A. J.; Credgington, D.; Pu, Y.-J.; Marderr, S. R.; Evans, E. W., Electron Spin Resonance Resolves Intermediate Triplet States in Delayed Fluorescence. *Nat. Commun.* **2021,** *12*, 4532.

(41) Fernando, B. D.; Thomas, J. P.; Andrew, P. M., Photophysics of Thermally Activated Delayed Fluorescence Molecules. *Methods and Applications in Fluorescence* **2017,** *5*, 012001.

(42) Zhang, X.; Fuentes-Hernandez, C.; Zhang, Y.; Cooper, M. W.; Barlow, S.; Marder, S. R.; Kippelen, B., High Performance Blue-Emitting Organic Light-Emitting Diodes from Thermally Activated Delayed Fluorescence: A Guest/Host Ratio Study. *J. Appl. Phys.* **2018,** *124*, 055501.

(43) Masui, K.; Nakanotani, H.; Adachi, C., Analysis of Exciton Annihilation in High-Efficiency Sky-Blue Organic Light-Emitting Diodes with Thermally Activated Delayed Fluorescence. *Org. Electron.* **2013,** *14*, 2721-2726.

Table of Contents artwork